Taylor & Francis
Taylor & Francis Group

Effect of evanescent channels on position-dependent diffusion in disordered waveguides

Ben Payne, Tom Mahler and Alexey G. Yamilov*

Department of Physics, Missouri University of Science & Technology, Rolla, MO, USA

We employ *ab initio* simulations of wave transport in disordered waveguides to demonstrate explicitly that although accounting for evanescent channels manifests itself in the renormalization of the transport mean free path, the position-dependent diffusion coefficient, as well as distributions of angular transmission, total transmission and conductance, all remain universal.

1. Introduction

Wave interference leads to deviations from the diffusive description of wave propagation through a random medium. This is a manifestation of an onset of Anderson localization – a paradigm in mesoscopic physics [1–3].

Self-consistent theory (SCT) of localization [4,5] accounts for the wave interference effects by renormalizing (reducing) the diffusion coefficient. In an experiment, one deals with samples of finite size. In such an open system, the SCT predicts [6–9] that the diffusion coefficient becomes position dependent. This is because the wave can escape through a boundary and hence reduce interference corrections.

Localization in finite media can be studied in quasi-one-dimension (quasi-1D) where the transition from diffusion to localization occurs with an increase in the system length [10]. A wire for an electronic system or a random waveguide as an optical counterpart are examples of quasi-1D systems. Position dependence of the diffusion coefficient has been demonstrated [11,12] in ab-initio numerical simulations of wave transport in a disordered waveguide.

Details of the microscopical disorder become evident in the near-field [13,14] and play an important role in the transport of the electromagnetic waves in random media [15]. The evanescent fields are an inseparable part of the quasi-modes of the open random media considered in transport geometry. In optical systems considered here, quasi-modes [16] are used to explain the effect of coherent random lasing [17–20]. Fluctuations of the local density of states [21–23] and the related spatial intensity correlations [24,25] carry information about near-fields; thus they are sensitive to the microscopical details of the disorder and are not universal. The position-dependent diffusion coefficient is defined as the ratio between local statistically averaged flux and the gradient of energy density. Because both of the latter two parameters should be smooth on the scales less than transport mean free path, the position

---

*Corresponding author. Email: yamilov@mst.edu

dependent diffusion is expected to be universal. In this work, we directly test this assumption in *ab initio* numerical simulations.

The quasi-1D geometry of a waveguide is useful for studying wave transport because quantization of the transverse component of momentum provides a convenient enumerable basis of channels leading to the transfer matrix description [26]. The component of the wave vector perpendicular to the direction of propagation is $k_{\perp\mu} = (\mu\pi)/w$, where w is the width of the waveguide, and μ is the channel index. The component of $\vec{k}$ parallel to the direction of propagation, $k_{\parallel\mu} = \sqrt{(\omega/c)^2 - (\mu\pi/w)^2}$, becomes imaginary for sufficiently large channel index $\mu > N_p$. Here ω is frequency, c is speed of light, and the width w is chosen such that the system is not close to a special case of $k_{\parallel N_p} = 0$.[27,28] N_p propagating channels with real-valued $k_{\parallel\mu}$ are "open" when the waveguide is empty, and the evanescent channels for which $k_{\parallel\mu}$ is imaginary are often referred to as "closed" because they do not carry a flux in an empty waveguide. This is the reason why these channels do not appear in the overall transmission matrix of the system.

Properly accounting for evanescent channels and coupling between scatterers induced by them [29] is a notoriously difficult problem. Commonly, evanescent channels are not considered explicitly, instead, a phenomenological parameter, transport mean free path, is introduced. This treatment is sufficient to describe the macroscopic wave transport as exemplified by the success of Dorokhov and Mello, Pereyra, and Kumar theory [29,30]. The evanescent channels were not included explicitly in random matrix theories until recently [31]. This treatment was justified by the so-called folding procedure [27,32] which allows one for *a single scatterer* to collapse the full $2(N_p + N_e) \times 2(N_p + N_e)$ transfer matrix to the smaller matrix $2N_p \times 2N_p$. Here, N_e is the number of evanescent channels in the transfer matrix and the factor two reflects a possibility of forward and backward propagation within each channel. This procedure is in line with the key concept in mesoscopic physics – universality [2] – only one (macroscopic) parameter survives when one is concerned with such transport properties as conductance. Some evidence for universality of position-dependent diffusion coefficient has been presented in Refs. [11,12]. Here, we study how evanescent channels affect the transport properties of the waveguide with volume disorder. We demonstrate that the position-dependent diffusion, as well as angular and the total transmission which are measurable in optical experiments, are all universal.

In Section 2, we describe a numerical model which has been used to obtain results in Ref. [11]. It describes a disordered medium as a collection of randomly placed scattering potentials in a planar quasi-1D metallic waveguide. The transfer matrix method is used [33–35], and self-embedding technique [36,37] is employed to control numerical errors in simulation. The number of propagating and evanescent channels, scattering strength, system dimensions, and scatterer density are adjustable parameters. The outcome of the numerical simulations is transmission and reflection matrices, and the electric fields throughout the volume of the waveguide. By varying the scatterer configuration, we obtain a large statistical ensemble. In Section 3, we show that including evanescent channels results in renormalization of the transport mean free path. Universality of the position-dependent diffusion coefficient, c.f. Section 4, as well as all transport parameters based on transfer matrix, is preserved. Therefore, one can always find an equivalent system with suitable parameters

where evanescent channels do not participate in transport and, hence, can be neglected in the simulations. This makes the computation numerically stable and allows modeling of much larger systems, such as those exhibiting Anderson localization [11].

In the appendix, we describe an algorithm for constructing a random potential which corresponds to a given scattering matrix.

2. Numerical model

Our goal is to perform *ab initio* numerical simulations without making any assumptions about the nature or strength of multiple-wave interference. We consider a scalar, monochromatic wave $E(\mathbf{r})e^{-i\omega t}$ propagating in a 2D volume-disordered waveguide of width w and length $L \gg w$. The wave field $E(\mathbf{r})$ obeys the 2D Helmholtz equation:

$$\left[\nabla^2 + k^2 (1 + \delta\epsilon(\mathbf{r}))\right] E(\mathbf{r}) = 0. \tag{1}$$

Here, $k = \omega/c$ is the wavenumber and $\delta\epsilon(\mathbf{r})$ is the randomly fluctuating part of the dielectric constant. The waveguide geometry considered here offers a convenient basis for description of wave propagation [26] because the transverse, y-axis, momentum is quantized $k_{\perp\mu} = \pi\mu/w$ with an integer μ. The transverse modes of the empty waveguide are $\chi_\mu(y) = (2/w)^{1/2} \sin(k_{\perp\mu} y)$. We represent $\delta\epsilon(\mathbf{r})$ as a collection of M randomly positioned "screens", scattering potentials $f(y, y_m)$, perpendicular to the z axis of the waveguide:

$$\delta\epsilon(\mathbf{r}) = \sum_{m=1}^{M} \alpha\delta(z - z_m) f(y, y_m), \tag{2}$$

where z_m represent random positions of the screens and α measures their scattering strength. A function $f(y, y_m)$, parametrized by random value y_m with $0 < y_m < w$, is to be determined below. The chosen form of random potential in Equation (2) allows us to express the electric field in the waveguide between two successive scattering planes $z_m < z < z_{m+1}$ as

$$E(y, z) = \sum_{\mu=1}^{N_p+N_e} \left[E_\mu^{(+)}(z_m)e^{ik_{\parallel\mu}(z-z_m)} \right.$$
$$\left. + E_\mu^{(-)}(z_m)e^{-ik_{\parallel\mu}(z-z_m)} \right] \chi_\mu(y). \tag{3}$$

$E_\mu^{(\pm)}(z_m)$ are the amplitudes of the forward and backward propagating components of the μ'th mode. $k_{\parallel\mu} = \left[k^2 - k_{\perp\mu}^2\right]^{1/2}$ is the longitudinal component of the momentum. For the propagating modes with $1 < \mu \leq N_p$, $k_{\parallel\mu}$ is real-valued, whereas for the evanescent ones $N_p < \mu \leq N_p + N_e$, $k_{\parallel\mu}$ becomes purely imaginary. The number of propagating channels N_p, an integer part of kw/π, depends on the width of the waveguide. Although the number of evanescent channels is not bound, in practice, a suitable N_e can be chosen based on the nature of scattering. This can be seen with the following argument. Substituting Equation (3) into Equation (1), we obtain
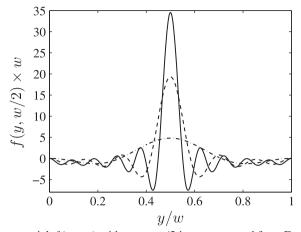
Figure 1. Random potential $f(y, y_m)$ with $y_m = w/2$ is reconstructed from Equation (6) using the procedure described in the Appendix. Dot-dash, dash, and solid lines correspond to $N_p + N_e = 2, 6, 10$ respectively. One can observe the convergence of $f(y, y_m) \rightarrow \delta(y - y_m)$ with an increase in $N_p + N_e$.

$$
E_{\mu}^{(\pm)}(z_{m+1}) = E_{\mu}^{(\pm)}(z_m)e^{\pm ik_{\|\mu}(z_{m+1}-z_m)} \mp \frac{k^2}{2ik_{\|\mu}} \times
$$
$$
\times \sum_{\nu=1}^{N_p+N_e} \Gamma_{\mu\nu}^{(m)} \left[E_{\nu}^{(+)}(z_m)e^{ik_{\|\nu}(z_{m+1}-z_m)} \right.
$$
$$
\left. + E_{\nu}^{(-)}(z_m)e^{-ik_{\|\nu}(z_{m+1}-z_m)} \right]. \tag{4}
$$

The process of scattering at the m's site is fully described by the matrix

$$
\Gamma_{\mu\nu}^{(m)} = \int\limits_{0}^{w} \alpha f(y, y_m)\chi_{\mu}(y)\chi_{\nu}(y)dy. \tag{5}
$$

Hence, by truncating the matrix as $\Gamma_{\mu\nu}^{(m)} \equiv 0$ for all $\mu, \nu > N_p + N_e$ one avoids excitation of these channels in the course of the scattering processes. In our model, we chose

$$
\Gamma_{\mu\nu}^{(m)} = \alpha\chi_{\mu}(y_m)\chi_{\nu}(y_m), \quad \mu, \nu \leq N_p + N_e. \tag{6}
$$

By comparing this expression to Equation (5), one can see that $f(y, y_m) \rightarrow \delta(y - y_m)$ in the limit $N_e \rightarrow \infty$. In the Appendix we describe the nontrivial mathematical procedure for finding the scattering potential for a given $\Gamma_{\mu\nu}^{(m)}$. Figure 1 depicts $f(y, y_m = w/2)$ for $\Gamma_{\mu\nu}^{(m)}$ given by Equation (6) with $N_p + N_e = 2, 6, 10$. Of course, to fully resolve a δ-function using the discrete channels would require accounting for infinitely many evanescent channels. By choosing proper scattering potentials rather than point scatterers, we are able to limit N_e and, by varying its value, to vary the microscopical properties of disorder, c.f. Figure 1.

When the special condition $k_{\|\mu=N_p} = 0$ is met, propagation can lead to some counter-intuitive phenomena in both electronic [38] and electromagnetic [39] transport. We avoid this degenerate case by setting $w = (N_p + 1/2)\lambda/2$. This choice of w puts kw/π exactly halfway between two successive integers N_p and $N_p + 1$.

As seen from Equation (4), the channel-indexed equations can be written as a system of linear equations. Thus, wave propagation can be described by matrices of rank $2(N_p + N_e)$ of two types: (i) free space matrices, and (ii) scattering matrices. These matrices are multiplied to form a total matrix which defines the transmission matrix $t_{\mu\nu}$ [40]. The latter describes the flux $T_{\mu\nu} = |t_{\mu\nu}|^2$ registered at channel $\mu \leq N_p$ if unit flux is launched into channel $\nu \leq N_p$. Total transmission $T_\mu = \sum_{\nu=1}^{N_p} T_{\mu\nu}$ is the total flux transmitted into all channels. Lastly, when unit flux is injected into each channel, the total transmitted flux is described by conductance $g = \sum_{\mu,\nu=1}^{N_p} T_{\mu\nu}$. Unlike the mesoscopic electronic transport, measurements of the electromagnetic wave transmission through a disordered waveguide allow measurement of all channel-resolved transmission coefficients [41].

The computation of the simple product of individual matrices is a straightforward approach to field propagation but is not numerically stable over many multiplications ($\sim 10^2$–10^5 for the results in this paper), as the eigenvalues in the product become divergent [42]. The deterioration caused by diverging eigenvalues is corrected by renormalizing the products. We implement a self-embedding procedure [43] to change the growth of error inherent in numerical matrix multiplication from exponential to linear. This allows us to limit the errors in flux conservation to less than 10^{-10} in all cases, which is critical as it allows the transfer matrix method to be used in the diffusive and localized (extremely long waveguides) regimes.

The system is excited from the left by illuminating the waveguide with N_p unit fluxes (one in each right propagating mode) and the wave field $E(\mathbf{r})$ is computed for a given realization of disorder. To compute statistical averages, ensembles of no fewer than 10^7 realizations are used in the results presented below.

3. Renormalization of transport mean free path

To estimate the transport mean free path ℓ in our model, we perform a set of simulations for different disorder strengths and waveguide lengths, exploring both the regime of classical diffusion $g_0 \equiv (\pi/2) N_p \ell / (L + 2z_0) \gg 1$ and that of Anderson localization $g_0 \ll 1$. $z_0 = (\pi/4)\ell$ is the so-called extrapolation length [43]. The dependencies of $\langle g \rangle$ and $\mathrm{var}(g)$ on g_0 are fitted by the analytic expressions obtained by Mirlin [44] using the supersymmetry approach with ℓ as the only fit parameter [11]. To distinguish between system with and without evanescent channels, we introduce an explicit dependence of the transport mean free path on the number of evanescent channels $\ell(N_e)$. We note that, strictly speaking, the transport mean free path in our model should depend on the total number of channels $N_p + N_e$, c.f. Figure 1.

To verify that the renormalizing effect of evanescent channels on transport mean free path does not affect SPS [10], the average conductance $\langle g \rangle$ and its variance are computed in numerical simulations of quasi-1D waveguides. Once $\langle g \rangle$ is known, SPS predicts that all other transport parameters are uniquely defined. Numerical results are compared to SPS predictions found with the supersymmetry approach [44]. When no evanescent channels are present in our numerical model, the simulation results obey SPS, c.f. Figure 2. No fitting parameters are used; the factor of $15/2$ is to account for the quasi-1D geometry of the waveguide. Although variance of the conductance distribution decreases deeper into the localization regime $\langle g \rangle \to 0$, c.f. Figure 2, its relative value $\mathrm{var}(g)/\langle g \rangle^2$ actually diverges. This is a manifestation of the lognormal distribution conductance in localized systems [30].
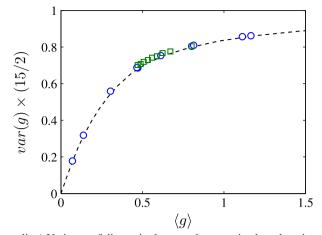
Figure 2. (Color online) Variance of dimensionless conductance is plotted vs. its mean value. Open circles represent numerically computed data for systems with $N_p = 10$, $N_e = 0$ and varying L. The dashed line plots Equation (6.23) of Ref. [44], derived using the supersymmetry approach. No fitting parameters are used. As per single parameter scaling (SPS), the variance of dimensionless conductance is uniquely determined by its average. Open squares represent the system with $L/\lambda = 200$, $N_p = 10$ and N_e from 0 to 8 evanescent channels in the right-to-left order. The effect of evanescent channels is to effectively reduce $\langle g \rangle$ or, in other words, to renormalize (decrease) $\ell(N_e)$ while retaining the property of SPS.

When a finite number of evanescent channels is added, c.f. Figure 2, the average conductance decreases. However, the relation between average conductance and its variance remains consistent with SPS since variance also decreases. As more evanescent channels are included, the ratio monotonically decreases. Again, no fitting parameters are needed.

There are two important observations from Figure 2. First, in our model the average conductance decreases when more evanescent channels are present because ℓ is renormalized as there are more channels available at each scatterer for incident waves to scatter into. Analytically, renormalization of $\ell(N_e)$ is accounted for by the folding procedure [31,38]. Thus macroscopical models that use ℓ as an input parameter, as well as numerical models that do not include evanescent channels, give adequate description of wave transport which is consistent with the SPS hypothesis.

Conformance of $\langle g \rangle$ and $var(g)$ with SPS, and our conclusion about the effective renormalization of $\ell(N_e)$ above, were based on the first two moments of conductance. To perform a more rigorous test, we find the entire distribution of conductance, as well as the distributions of total and channel-resolved transmission, using the numerical model, c.f. Figure 3. When evanescent channels are included for a given waveguide geometry, the entire distribution changes. However, the system which includes evanescent channels has the same distribution as another waveguide with with the equivalent value of g_0 and $N_e = 0$. Effectively, the presence of evanescent channels is equivalent to increasing system length to L' so that optical depth is the same in both cases $L/\ell(N_e) = L'/\ell(0)$. One can see that this condition of equivalence means that $g_0 = (\pi/2)N_p\ell(N_e)/[L + (\pi/2)\ell(N_e)] = (\pi/2)N_p\ell(0)/[L' + (\pi/2)\ell(0)]$.
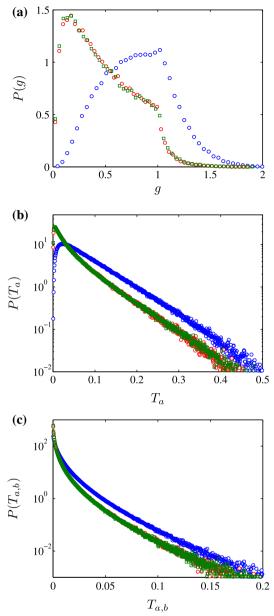
Figure 3. (Color online) Panel (a) shows the distribution of dimensionless conductance $P(g)$ for three waveguides, each with 10 propagating channels. $P(g)$ from the numerical simulation of waveguide with length $L/\lambda = 200$ and no evanescent channels, blue open circles, is significantly distinct from $P(g)$ for the same geometry and $N_e = 8$ evanescent channels, green squares. However, the system with evanescent channels is equivalent to a longer system, $L'/\lambda = 300$, with an equivalent value of L/ℓ - red open circles. Hence, the only effect of inclusion of evanescent channels is to renormalize $\ell(N_e)$. Panels (b,c) demonstrate that this argument also applies to $P(T_a)$ and $P(T_{ab})$, respectively.
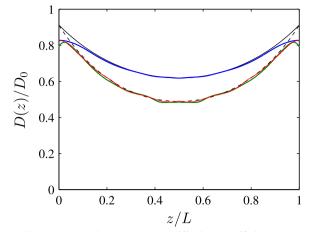
Figure 4. (Color online) (a) Position-dependent diffusion coefficient $D(z)/D_0$ for the three geometries shown in each of the panels in Figure 3. The diffusion coefficient for two microscopically different samples ($N_e = 8$ – green and $N_e = 0$ – red solid lines) coincides because they both have identical value of L/ℓ hence confirming the universality of $D(z)$. The result of SCT is shown as solid and dashed black lines for two values of L/ℓ. Numerical simulations and SCT agree without fitting in both cases with exception of two boundary regions.

4. Position-dependent diffusion coefficient

The wave amplitude $E_\mu^{(\pm)}(z_m)$ of each channel that we obtain from the numerical algorithm allows us to calculate the energy density $\mathcal{W}(z)$ and the longitudinal component of flux $J_z(z)$ [45]:

$$\mathcal{W}(z_m) = k^2 \sum_{\mu=1}^{N_p+N_e} \left[\left| E_\mu^{(+)}(z_m) \right|^2 + \left| E_\mu^{(-)}(z_m) \right|^2 \right], \tag{7}$$

$$J_z(z_m) = k \sum_{\mu=1}^{N_p} k_{\|\mu} \left[\left| E_\mu^{(+)}(z_m) \right|^2 - \left| E_\mu^{(-)}(z_m) \right|^2 \right]. \tag{8}$$

These two quantities formally define the diffusion coefficient $D(z)$ which, in general, may be position-dependent:

$$D(z) = -\langle J_z(z) \rangle / \left[d \langle \mathcal{W}(z) \rangle / dz \right], \tag{9}$$

where the averages $\langle \ldots \rangle$ are taken over a statistical ensemble of disorder realizations.

In order to compare our numerical results for $D(z)$ with self-consistent theory (SCT) without fitting parameters, we need to obtain the value of the diffusion coefficient unrenormalized by the wave interference effects $D_0 = v\ell/2$. The numerical procedure for obtaining the transport mean free path has been described in Section 3 above. To find the diffusive speed v, we use the definition of diffusive flux resolved with respect to the direction of propagation [45]

$$\langle J_z^{(\pm)}(z) \rangle = (v/4) \langle \mathcal{W}(z) \rangle \mp (D(z)/2) d \langle \mathcal{W}(z) \rangle / dz, \tag{10}$$

where $J_z^{(\pm)}(z)$ represent the forward (plus) and backward (minus) propagating components of the flux. These two quantities are found as the first and second term in Equation (8). Combining the two components, we find

$$v = 2 \left(\langle J_z^{(+)}(z) \rangle + \langle J_z^{(-)}(z) \rangle \right) / \langle \mathcal{W}(z) \rangle. \tag{11}$$

Unlike $D(z)$ defined by Equation (9), we numerically find that the diffusive speed in Equation (11) does not change with z with exception of small boundary regions $z \lesssim \ell$ and $z \gtrsim L - \ell$.

Figure 4 plots $D(z)/D_0$ computed numerically for the three geometries shown in each panel of Figure 3 using the same color scheme – as blue, green, and red lines. Two microscopically different samples ($L/\lambda = 200$, $N_e = 8$ and $L/\lambda = 300$, $N_e = 0$) with the identical values of L/ℓ have the same position-dependent diffusion coefficient (green and red lines) throughout the bulk of the system. We stress that the agreement is achieved with no fitting parameters. The discrepancy between the two systems observed in the immediate vicinity of the boundaries of the system. We attribute this nonuniversality to the boundary effect which depends on the details the wave propagation near the surface, including surface reflections[43], and hence is sensitive to the microscopical disorder.

Now we formally introduce SCT formalism for position-dependent diffusion. In quasi-1D waveguides $d(z) = D(z)/D_0$ is obtained following the approach of Refs. [9,11]:

$$\frac{\partial}{\partial \zeta} d(\zeta) \frac{\partial}{\partial \zeta} \hat{C}(\zeta, \zeta') = \delta(\zeta - \zeta'), \tag{12}$$

$$\frac{1}{d(\zeta)} = 1 + \frac{2}{\tilde{g}_0} \hat{C}(\zeta, \zeta). \tag{13}$$

Here, the function $\hat{C}(\zeta, \zeta')$ is related to the Green's function of the original wave equation, Equation (1); $D_0 = v\ell/2$ is the Boltzmann diffusion coefficient, $\zeta = z/L$ is the dimensionless position coordinate, and $\tilde{g}_0 = (\pi/2)N_p\ell/L$. These equations should be solved with the following boundary conditions:

$$\hat{C}(\zeta, \zeta') \mp \frac{z_0}{L} d(\zeta) \frac{\partial}{\partial \zeta} \hat{C}(\zeta, \zeta') = 0 \tag{14}$$

at $\zeta = 0$ and $\zeta = 1$. When Equations (12–14) are solved in the diffuse regime $\tilde{g}_0 \gg 1$, the dimensionless conductance of the waveguide is found to be $g_0 = (\pi/2)N\ell/(L + 2z_0)$ [30,43] which is close to $\tilde{g}_0$ for $z_0 \ll L$.

The solid and dashed black lines in Figure 4 are found for values of L/ℓ which are known from numerical simulations. For both values of L/ℓ, the SCT result agrees with numerical simulations with no fitting parameters. The nonuniversal (disorder-dependent) deviation from SCT is confined to the immediate vicinity to the boundaries. It is known [45] that a diffusion description, such as SCT, is not sufficiently accurate on distances shorter than about one transport mean free path ℓ from the boundaries of the random medium, where a more sophisticated description using the Milne equation [46] is required.

5. Conclusion

In this work, we obtained three main results. First, using a numerical transfer-matrix model of quasi-1D waveguides with densely packed, randomly placed scatterers the effect of

evanescent channels on conductivity was simulated. The number of matrices multiplied is limited by numerical accuracy, and has been extended using self-embedding technique. This procedure is so robust to numerical errors that calculations remain accurate even when transfer matrices include a finite number of evanescent channels. However, due to the fact that free-space matrices including evanescent channels contain exponentially diverging eigenvalues, the numerically intensive self-embedding steps have to be performed more often. This slows down numerical simulations dramatically, so it is desirable to avoid the evanescent channels altogether.

The simulations presented in this work demonstrate that evanescent channels of the waveguide can be neglected. Indeed, although inclusion of the evanescent channels in our model leads to (i) the additional mechanism of coupling between scatterers and (ii) change the microscopical properties of the scatterers, the universality of wave transport is preserved. This allows us to find an equivalent system (exhibiting the same statistical and transport properties) without evanescent channels.

Secondly, we explicitly demonstrate that the position-dependent diffusion coefficient introduced in the SCT of localization is a universal quantity throughout the bulk of the random medium. The nonuniversal behavior of $D(z)$ is confined to the immediate vicinities of the boundaries that extend to a distance on the order one transport mean free path. We attribute these deviations to the disorder-dependent reflections from the interface of random medium and the surrounding free space.

The third result is obtained in the appendix. We develop a mathematical procedure to construct the disorder potential from a given scattering matrix. In the context of the present work, this method demonstrates the change of the microscopical disorder in our model when a different number of evanescent channels is included in calculations. However, our method can be applied to a general problem of constructing a disorder potential for a given scattering matrix.

Acknowledgements

References

[1] Anderson PW. Absence of diffusion in certain random lattices. Phys. Rev. 1958;109:1492–1505.
[2] Altshuler BL, Lee PA, Webb RA, editors. Mesoscopic phenomena in solids. Amsterdam: North-Holland; 1991.
[3] Abrahams E, editor. Fifty years of Anderson localization. Singapore: World Scientific; 2010.
[4] Vollhardt D, Wölfle P. Diagrammatic, self-consistent treatment of the Anderson localization problem in d=2 dimensions. Phys. Rev. B. 1980;22:4666–4679.
[5] Kroha J, Soukoulis CM, Wölfle P. Localization of classical waves in a random medium: a self-consistent theory. Phys. Rev. B. 1993;47:11093–11096.
[6] van Tiggelen BA, Lagendijk A, Wiersma DS. Reflection and transmission of waves near the localization threshold. Phys. Rev. Lett. 2000;84:4333–4336.
[7] Skipetrov SE, van Tiggelen BA. Dynamics of weakly localized waves. Phys. Rev. Lett. 2004;92:113901.

[8] Skipetrov SE, van Tiggelen BA. Dynamics of Anderson localization in open 3D media. Phys. Rev. Lett. 2006;96:043902.

[9] Cherroret N, Skipetrov SE. Microscopic derivation of self-consistent equations of Anderson localization in a disordered medium of finite size. Phys. Rev. E. 2008;77:046608.

[10] Abrahams E, Anderson PW, Licciardello DC, Ramakrishnan TV. Scaling theory of localization: Absence of quantum diffusion in two dimensions. Phys. Rev. Lett. 1979;42:673–676.

[11] Payne B, Yamilov A, Skipetrov SE. Anderson localization as position-dependent diffusion in disordered waveguides. Phys. Rev. B. 2010;82:024205.

[12] Tian C, Cheung S, Zhang Z. Local diffusion theory for localized waves in open media. Phys. Rev. Lett. 2010;105:263905.

[13] Apostol A, Dogariu A. Spatial correlations in the near field of random media. Phys. Rev. Lett. 2003;91:093901.

[14] Joulain K, Carminati R, Mulet JP, Greffet JJ. Definition and measurement of the local density of electromagnetic states close to an interface. Phys. Rev. B. 2003;68:45405.

[15] Shapiro B. New type of intensity correlation in random media. Phys. Rev. Lett. 1999;83:4733–4735.

[16] Wang J, Genack AZ. Transport through modes in random media. Nature. 2011;471:345–348.

[17] Cao H. Review on latest developments in random lasers with coherent feedback. J. Phys. A: Math. Gen. 2005;38:10497–10535.

[18] Yamilov A, Wu X, Cao H, Burin AL. Absorption-induced confinement of lasing modes in diffusive random media. Opt. Lett. 2005;30:2430–2432.

[19] Tureci HE, Ge L, Rotter S, Stone AD. Strong interactions in multimode random lasers. Science. 2008;320:643–646.

[20] Hackenbroich G. Statistical theory of multimode random lasers. J. Phys. A. 2005;38:10537–10543.

[21] Asatryan AA, Busch K, McPhedran RC, Botten LC, de Sterke CM, Nicorovici NA. Two-dimensional Greens function and local density of states in photonic crystals consisting of a finite number of cylinders of infinite length. Phys. Rev. E. 2001;63:046612.

[22] Boriskina SV, Gopinath A, Negro LD. Optical gaps, mode patterns and dipole radiation in two-dimensional aperiodic photonic structures. Physica E. 2009;41:1102–1106.

[23] Birowosuto MD, Skipetrov SE, Vos WL, Mosk AP. Observation of spatial fluctuations of the local density of states in random photonic media. Phys. Rev. Lett. 2010;105:013904.

[24] van Tiggelen BA, Skipetrov SE. Fluctuations of local density of states and C0 speckle correlations are equal. Phys. Rev. E. 2006;73:045601.

[25] Cazé A, Pierrat R, Carminati R. Near-field interactions and nonuniversality in speckle patterns produced by a point source in a disordered medium. Phys. Rev. A. 2010;82:043823.

[26] Mello PA, Kumar N. Quantum Transport in Mesoscopic Systems. Oxford: Oxford University Press; 2004.

[27] Kumar A, Bagwell PF. Resonant tunneling in a quasi-one-dimensional wire: influence of evanescent modes. Phys. Rev. B. 1991;43:9012–9020.

[28] Edwards B, Alu A, Young M, Silveirinha M, Engheta N. Experimental verification of epsilon-near-zero metamaterial coupling and energy squeezing using a microwave waveguide. Phys. Rev. Lett. 2008;10:033903.

[29] Gómez-Medina R, Sáenz JJ. Unusually strong optical interactions between particles in quasi-one-dimensional geometries. Phys. Rev. Lett. 2004;93:243602.

[30] Beenakker CW. Random-matrix theory of quantum transport. Rev. Mod. Phys. 1997;69:731–808.

[31] Froufe-Pérez LS, Yépez M, Mello PA, Sáenz JJ. Statistical scattering of waves in disordered waveguides: From microscopic potentials to limiting macroscopic statistics. Phys. Rev. E. 2007;75:031113.

[32] Froufe-Pérez LS, Yépez M, Mello PA, Sáenz JJ. Transport of waves in disordered waveguides: a potential model. Physica A. 2007;386:603–610.

[33] MacKinnon A, Kramer B. One-parameter scaling of localization length and conductance in disordered systems. Phys. Rev. Lett. 1981;47:1546–1549.

[34] Pendry JB, MacKinnon A. Calculation of photon dispersion relations. Phys. Rev. Lett. 1992;69:2772–2775.

[35] Brandes T, Kettemann S. Anderson localization and its ramifications. Berlin: Springer; 2003.

[36] Deych LI, Yamilov A, Lisyansky AA. Effects of resonant tunneling in electromagnetic wave propagation through a polariton gap. Phys. Rev. B. 1999;59:11339–11348.

[37] Bellman R, Wing G. An Introduction to Invariant Embedding. New York, NY: Wiley; 1976.

[38] Bagwell PF. Evanescent modes and scattering in quasi-one-dimensional wires. Phys. Rev. B. 1990;41:10354–10371.

[39] Silveirinha M, Engheta N. Tunneling of electromagnetic energy through subwavelength channels and bends using epsilon-near-zero materials. Phys. Rev. Lett. 2006;97:157403.

[40] Yamilov A. Relation between channel and spatial mesoscopic correlations in volume-disordered waveguides. Phys. Rev. B. 2008;78:045104.

[41] Genack AZ, Chabanov AA. Signatures of photon localization. J. Phys. A. 2005;38:10465–10488.

[42] Osedelec VI. A multiplicative ergodic theorem: Lyapunov characteristic exponents for dynamical systems. Trans. Mosc. Math. Soc. 1968;19:197–231.

[43] van Rossum MC, Nieuwenhuizen TM. Multiple scattering of classical waves: Microscopy, mesoscopy, and diffusion. Rev. Mod. Phys. 1999;71:313–371.

[44] Mirlin A. Transmission coefficient and the localization length of an electron in N bound disordered chains. Phys. Rep. 2000;326:259–262.

[45] Morse PM, Feshbach H. Methods of theoretical physics. New York, NY: McGraw-Hill; 1953.

[46] Akkermans E, Montambaux G. Mesoscopic physics of electrons and photons. Cambridge: Cambridge University Press; 2007.

Appendix: Reconstruction of random potential

Below we describe the procedure to invert Equation (5) and find the function $f(y, y_m)$. In particular, we obtain the result shown in Figure 1 in the case when $\Gamma_{\mu\nu}^{(m)}$ is given by Equation (6). To simplify the notations in the derivation below, we assume summations over the repeated indices from 1 to $N_p + N_e$.

First, we represent the unknown function as

$$\alpha f(y, y_m) = \alpha_{\mu'\nu'}^{(m)} \chi_{\mu'}(y) \chi_{\nu'}(y). \tag{15}$$

Our goal is to find the coefficients $\alpha_{\mu'\nu'}^{(m)}$. Substituting Equation (15) into Equation (5) we obtain

$$\Gamma_{\mu\nu}^{(m)} = \mathfrak{S}_{\mu\nu,\mu'\nu'} \alpha_{\mu'\nu'}^{(m)}, \tag{16}$$

where

$$\mathfrak{S}_{\mu\nu,\mu'\nu'} = \frac{1}{2(N_p + N_e)} \sum_{\mu'\nu'=1}^{N_p+N_e} \left(\delta_{\mu+\nu+\mu'+\nu'} - \right. \tag{17}$$
$$\delta_{-\mu+\nu-\mu'-\nu'} - \delta_{\mu-\nu+\mu'+\nu'} - \delta_{\mu+\nu-\mu'+\nu'} - \delta_{\mu+\nu+\mu'-\nu'} +$$
$$\left. \delta_{\mu+\nu-\mu'-\nu'} + \delta_{\mu-\nu+\mu'-\nu'} + \delta_{\mu-\nu-\mu'+\nu'} \right)$$

and $\delta_\mu \equiv \delta_{\mu,0}$ is the Kronecker delta. The tensor $\mathfrak{S}_{\mu\nu,\mu'\nu'}$ can be represented as a matrix of size $(N_p + N_e)^2 \times (N_p + N_e)^2$. For $(N_p + N_e) > 1$ this matrix is singular, $\det \mathfrak{S}_{\mu\nu,\mu'\nu'} = 0$, and cannot be inverted to obtain $\alpha_{\mu'\nu'}^{(m)}$ from $\Gamma_{\mu\nu}^{(m)}$ because the inverse matrix cannot be defined.

If the matrix of a system of linear equations such as that in Equation (16) is singular, the system does not have a *unique* solution. This however does not preclude the existence of a family of *degenerate* solutions. To find these solutions we use the Moore–Penrose inverse, also called the pseudo-inverse, matrix $\mathfrak{S}^{+}_{\mu\nu,\mu'\nu'}$:

$$\alpha^{(m)}_{\mu\nu} = \mathfrak{S}^{+}_{\mu\nu,\mu'\nu'}\Gamma^{(m)}_{\mu'\nu'} + \left(\hat{I} - \mathfrak{S}^{+}_{\mu\nu,\rho\sigma}\mathfrak{S}_{\rho\sigma,\mu'\nu'}\right)\mathfrak{D}_{\mu'\nu'}, \tag{18}$$

where $\hat{I}$ is the identity matrix of size $\left(N_p + N_e\right)^2 \times \left(N_p + N_e\right)^2$ and $\mathfrak{D}_{\mu'\nu'}$ is *arbitrary*, reflecting the possibility of multiple solutions of Equation (16). Multiple solutions exist if and only if $\Gamma^{(m)}_{\mu'\nu'}$ satisfies the following condition

$$\mathfrak{S}_{\mu\nu,\rho\sigma}\mathfrak{S}^{+}_{\rho\sigma,\mu'\nu'}\Gamma^{(m)}_{\mu'\nu'} = \Gamma^{(m)}_{\mu\nu}. \tag{19}$$

The solution which corresponds to $\mathfrak{D}_{\mu'\nu'} \equiv 0$ is a special solution which has the least norm. The number of independent parameters in $\mathfrak{D}_{\mu'\nu'}$ that can be used in constructing other solutions is determined by the dimension of the null space of the matrix $\mathfrak{S}_{\mu\nu,\mu'\nu'}$.

In our case, $\Gamma^{(m)}_{\mu\nu}$ is given by Equation (6). This expression indeed satisfies Equation (19) and, hence, $\alpha^{(m)}_{\mu\nu}$ and $f(y, y_m)$ can be found. Figure (1) shows $f(y, y_m = w/2)$ for $N_p + N_e = 2, 6, 10$ for $\mathfrak{D}_{\mu'\nu'} \equiv 0$. One can see convergence to the delta function $\delta(y - y_m)$ with an increase in $N_p + N_e$ as required by Equations (5,6).